Three-dimensional vortex solitons in quasi-two-dimensional lattices

Hervé Leblond,[1] Boris A. Malomed,[2] and Dumitru Mihalache[3]
[1]*Laboratoire POMA, UMR 6136, Université d'Angers, 2 Bd Lavoisier, 49000 Angers, France*
[2]*Department of Physical Electronics, School of Electrical Engineering, Faculty of Engineering, Tel Aviv University, Tel Aviv 69978, Israel*
[3]*Department of Theoretical Physics, Horia Hulubei National Institute for Physics and Nuclear Engineering (IFIN-HH), 407 Atomistilor, Magurele-Bucharest 077125, Romania*
(Received 12 June 2006; published 17 August 2007)

We consider the three-dimensional (3D) Gross-Pitaevskii or nonlinear Schrödinger equation with a quasi-2D square-lattice potential (which corresponds to the optical lattice trapping a self-attractive Bose-Einstein condensate, or, in some approximation, to a photonic-crystal fiber, in terms of nonlinear optics). Stable 3D solitons, with embedded vorticity $S=1$ and 2, are found by means of the variational approximation and in a numerical form. They are built, basically, as sets of four fundamental solitons forming a rhombus, with phase shifts $\pi S/2$ between adjacent sites, and an empty site in the middle. The results demonstrate two species of stable 3D solitons, which were not studied before, viz., localized vortices ("spinning light bullets," in terms of optics) with $S>1$, and vortex solitons (with any $S\neq 0$) supported by a lattice in the 3D space. Typical scenarios of instability development (collapse or decay) of unstable localized vortices are identified too.

DOI: 10.1103/PhysRevE.76.026604 PACS number(s): 05.45.Yv, 42.65.Tg, 03.75.Lm

I. INTRODUCTION

The nonlinear Schrödinger equation (NLSE), alias the Gross-Pitaevskii equation (GPE) with self-focusing cubic nonlinearity, which describe, respectively, the light propagation in dispersive Kerr-nonlinear media, and evolution of the mean-field wave function in a Bose-Einstein condensate (BEC) with attraction between atoms, give rise to the wave collapse in two- and three-dimensional (2D and 3D) geometry, which makes the respective multidimensional solitons unstable [1]. It has been established that, nevertheless, multidimensional solitons can be stabilized by means of a periodic [3–6] or quasiperiodic [7] cellular potential added to the model. In the GPE, the potential represents an *optical lattice* (OL), which can be induced by pairs of counterpropagating coherent laser beams illuminating the condensate [2]. The OL may have 1D, 2D, or 3D shape, including the case of a *low-dimensional lattice*, which is represented by a cellular potential that does not depend on one coordinate, i.e., a quasi-1D (Q1D) or quasi-2D (Q2D) OL in the 2D or 3D space, respectively [5,6]. Generally, the OL whose dimension is less than the full spatial dimension by one can stabilize a soliton, but a 1D lattice cannot stabilize 3D solitons (without additional ingredients, such as *nonlinearity management* [8,9]); in addition, it has been predicted that a Q2D radial (axisymmetric) lattice, that can be induced by a nondiffracting Bessel light beam illuminating the BEC, supports stable 3D solitons [10]. The stabilization of solitons in these settings was explained by means of the *Vakhitov-Kolokolov* (VK) *criterion* (see below), and corroborated in direct simulations. An advantage of dealing with multidimensional solitons in low-dimensional lattices is that they can freely move in the unconfined direction, which opens a way to study their collisions in a common potential channel, or in adjacent ones [5].

The physical significance of the prediction of stable solitons is that it suggests a way to create persistent matter-wave pulses in the 2D and 3D space; thus far, they were only created in nearly 1D ("cigar-shaped") traps [11] (although the actual shape of the soliton may be nearly three dimensional [12]). Another, although less straightforward, physical realization of the Q2D lattice in the effectively 3D space is offered by photonic-crystal fibers (PCFs) fabricated in a Kerr-nonlinear material. Spatial (i.e., two-dimensional) solitons in this setting, localized in the transverse plane, were predicted in Refs. [13]. A fully localized spatiotemporal soliton, i.e., a 3D one (alias "light bullet"), may also be expected in PCFs, taking into regard that the anomalous group-velocity dispersion (GVD), necessary for the existence of temporal solitons (those localized along the fiber's axis), is possible in PCF [14]. However, the NLSE including a Q2D lattice potential is less accurate as a PCF model than the similar GPE as a model of BEC [see Eq. (1) below], because the PCF structure implies, in addition to the cellular transverse potential, spatial modulation of the local nonlinearity in the transverse directions, as there is no nonlinearity in voids running parallel to the fiber's axis.

Besides the fundamental 2D solitons, their counterparts carrying a topological charge (vorticity, alias *spin*, S) were also predicted, both in the GPE with the cellular potential [3,4], and as spatial solitons in the PCF [15]. It should be stressed that the model with the cellular potential has no rotational invariance, hence it does not conserve the angular momentum; nevertheless, the intrinsic soliton's vorticity, while not being related to any dynamical invariant, can be unambiguously defined as $\Phi/(2\pi)$, where Φ is the total change of the phase of the wave function along a closed path surrounding the vortex's center. Until very recently, stable 2D lattice solitons were only predicted with $S=1$ [3,4,15] (experimentally, they were created, also solely with $S=1$, in photorefractive crystals with a photonic lattice, which corresponds to saturable nonlinearity [16]). A new result is that the lattice potential supports stable higher-order vortex solitons (at least, up to $S=6$), multipoles (topologically orga-

 ©2007 The American Physical Society

nized solitary-wave patterns without vorticity), and *supervortices* (ring-shaped chains formed by compact vortices, each with $S=1$, carrying a global vorticity imprinted on top of the entire chain, i.e., 2D patterns characterized by mutually independent *local* and *global* vorticities) [17].

The objective of the present work is to construct *three-dimensional* vortex solitons, in the GPE with the Q2D lattice potential, which will extend both the recently reported results for the stable 3D solitons of the fundamental type ($S=0$) in the same setting [5,6], and the above-mentioned lattice-supported vortex solitons in two dimensions [3,4]. Note that, in models without the cellular potential, stabilization of 3D (and 2D) vortex solitons is only possible by means of competing nonlinearities, such as self-focusing cubic and defocusing quintic [18], or quadratic (second-harmonic-generating) and self-defocusing cubic terms [19]. Thus far, a stability region in these models was not found for 3D solitons with the spin other than $S=0$ and $S=1$ (see review [20]). In this paper, we demonstrate that the Q2D lattice allows the stabilization of localized vortices with (at least) $S=1$ and $S=2$ (the stability of the corresponding solitons with $S=0$ was established before [5,6]), in the usual cubic GPE. In this connection, it is relevant to mention that stable discrete solitons with embedded vorticity $S=1$ and 3, as well as stable quadrupoles and octupoles, have been reported in the 3D *discrete* NLS equation [21].

The stability of localized 3D vortices in the Q2D lattice is a challenge, rather than a straightforward extension of previously obtained results for the solitons with $S=0$ in the same model [5,6], and for vortex solitons in the 2D model with the 2D lattice [3,4,17]. Indeed, it is known in terms of the 2D model, and will be shown below in the 3D GPE with the Q2D lattice potential, that the vortex soliton is built, roughly speaking, as a set of four fundamental solitons (density peaks), trapped in four potential wells, which form a rhombus, with an empty site in the middle. The vorticity (S) is manifested by phase shifts between adjacent peaks $\Delta\Phi=(2\pi S)/4$ (see Figs. 9 and 12 below). It is well known too that the interaction between fundamental multidimensional solitons is attractive for $0\leqslant\Delta\Phi<\pi/2$, and repulsive for $\pi/2<\Delta\Phi\leqslant\pi$ [for vortex solitons, the interaction sign is additionally multiplied by $(-1)^S$] [22]. It is also known that the interplay of the interaction between solitons and their pinning by the lattice potential may give rise to *stable* bound states if the direct interaction is *repulsive* [23]. The latter argument explains quite well the stability and instability of higher-order vortices and supervortices supported by the 2D lattice in 2D equations, even if the stability of the vortex with $S=1$, corresponding to $\Delta\Phi=\pi/2$, seems indefinite, in this sense. In the 3D equation with the Q2D lattice potential, the same argument gives rise to a problem, as the repulsion between fundamental solitons, which constitute the vortex pattern, while helping to stabilize it in the lattice's plane, seem to make it unstable in the orthogonal (free) direction. It will be demonstrated below that stable 3D vortices with $S=1$ and $S=2$ can be found, nevertheless (that is, these qualitative arguments do not apply in all cases).

The paper is organized as follows. In the next section, we formulate the model and present analytical predictions for the vortex solitons and their stability obtained by means of the variational approximation (VA) and VK criterion. In Sec. III, we introduce numerical methods used in this work (a special two-stage numerical technique was developed, which makes it possible to find a 3D vortex-soliton solution with high accuracy), and then report basic numerical results. In particular, we demonstrate that most 3D vortex solitons are stable, although the stability region is limited. Generally, the numerical findings for the solitons with $S=1$ comply with the VA (the agreement may be considerably improved by means of a phenomenological linear adjustment of plots generated by the VA). Numerical results for $S=2$ vortices reveal a respective stability region too, but they are quite different from the predictions obtained by means of the VA in that case.

Numerical findings are presented below as sets of examples, as collecting results of direct simulations of the 3D model in a completely systematic form is really difficult. However, the examples will provide for adequate understanding of the generic situation.

A. Model and variational approximation

As said above, we aim to consider the GPE with the self-attractive cubic nonlinearity in the 3D space (x,y,z). The equation contains the Q2D square-shaped lattice potential, with strength $-\varepsilon$, whose period is scaled to be π. In normalized units, the GPE for the single-atom wave function u is [5,6]

$$i\frac{\partial u}{\partial t}+\left[\frac{1}{2}\left(\frac{\partial^2}{\partial x^2}+\frac{\partial^2}{\partial y^2}+\frac{\partial^2}{\partial z^2}\right)-\varepsilon(\cos(2x)+\cos(2y))+|u|^2\right]u=0. \tag{1}$$

In terms of nonlinear optics, the same equation with time t replaced by propagation distance z, and the third coordinate z replaced by the local time $\tau=t-z/V_0$ (V_0 is the group velocity of the carrier wave), describes the transmission of a spatiotemporal light signal in the bulk medium with the Kerr self-focusing nonlinearity, anomalous GVD, and transverse periodic modulation of the local refractive index.

Stationary solutions to Eq. (1) are looked for as $u=\psi(x,y,z)e^{-i\mu t}$, with chemical potential μ (in optics, $-\mu$ is the propagation constant). The equation for the stationary function ψ, which follows from Eq. (1), is associated with Lagrangian $L=\int\int\int\mathcal{L}dxdydz$, whose density is

$$\mathcal{L}=\frac{1}{2}(|\partial_x\psi|^2+|\partial_y\psi|^2+|\partial_z\psi|^2)+\varepsilon(\cos(2x)+\cos(2y))|\psi|^2-\frac{1}{2}|\psi|^4-\mu|\psi|^2. \tag{2}$$

The Hamiltonian associated with Eq. (1) (BEC energy) is $H=\int\int\int\mathcal{H}dxdydz$, with

$$\mathcal{H}=\frac{1}{2}(|\partial_x\psi|^2+|\partial_y\psi|^2+|\partial_z\psi|^2)+\varepsilon(\cos(2x)+\cos(2y))|\psi|^2-\frac{1}{2}|\psi|^4. \tag{3}$$

Along with the energy, the GPE conserves the norm, which

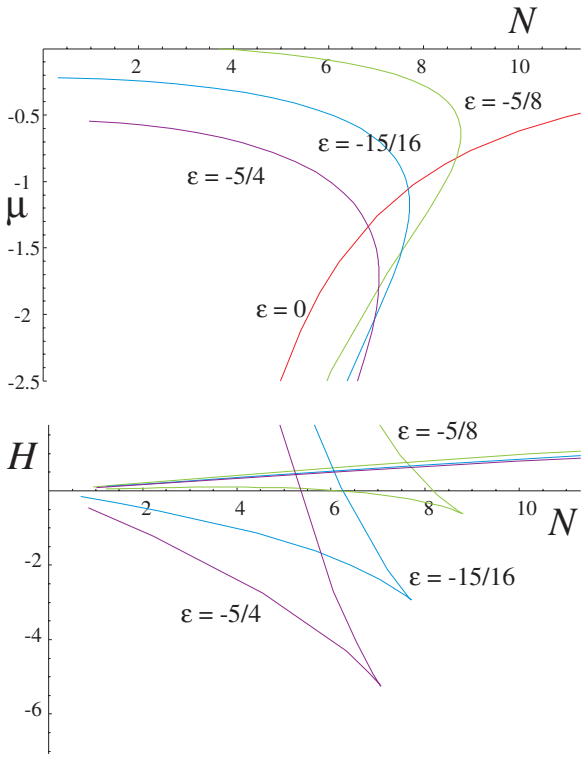

FIG. 1. (Color online) Dependences $\mu(N)$ (a) and $H(N)$ for the family of 3D solitons with $S=0$, as predicted by the variational approximation at several different values of strength ε of the quasi-2D lattice.

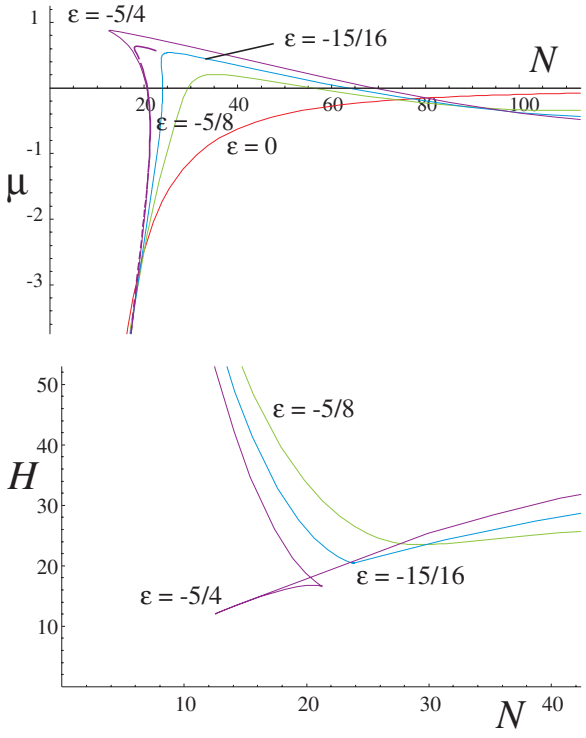

FIG. 2. (Color online) The same as in Fig. 1 for vortex solitons with $S=1$. In (a), the dashed curve additionally shows the $\mu(N)$ dependence as predicted by the modified approximation, based on ansatz (5), for $\varepsilon=-1.25$. Note a "swallow-tail" pattern in the $H(N)$ dependence, characteristic to models of this type [6,10].

is proportional to the number of atoms in BEC, or the total energy in terms of the optical model, $N=\int\int\int|\psi(x,y,z)|^2 \times dxdydz$.

We attempt to approximate 3D soliton solutions of Eq. (1), with vorticity $S=0,1,2,\ldots$, by the following *ansatz*:

$$\psi_S = A(x+iy)^S \exp\left(-\frac{x^2+y^2}{2\rho^2}-\frac{z^2}{2h^2}\right), \tag{4}$$

with real variational parameters A, ρ, and h [since $(x+iy)^S \equiv r^S e^{iS\theta}$, where r and θ are the polar coordinates in the plane of (x,y), the ansatz complies with the usual definition of the vorticity]. Following the general scheme of the VA [9,24], we substitute the ansatz in density (2) and calculate, in an analytical form, the effective Lagrangian. Then, the variational equations $dL/d\rho=dL/dh=dL/dA=0$ take a form, which makes it possible to solve them for A, h, and μ, treating ρ and ε as free parameters (i.e., ρ plays the role of an intrinsic parameter of the soliton family).

The results of the VA for $S=0$ and $S=1$ are presented, in the form of $\mu(N)$ and $H(N)$ dependences, in Figs. 1 and 2. In fact, the VA for the fundamental 3D solitons in the same model, based on ansatz (4), was elaborated in Ref. [5]. Here we include the variational results for $S=0$ for the sake of comparison with the new results pertaining to $S=1$.

The $\mu(N)$ dependence makes it possible to check the necessary stability condition given by the above-mentioned VK criterion $d\mu/dN<0$ [1,25]. Figures 1(a) and 2(a) demonstrate that the soliton families are correctly predicted to be VK unstable without the OL, $\varepsilon=0$, but contain segments that may be stable at $\varepsilon<0$. The VK criterion may only guarantee the absence of *real* unstable eigenvalues in the spectrum of small perturbations around the soliton, but it does not detect complex eigenvalues accounting for oscillatory instabilities. Indeed, in models with the quadratic or saturable nonlinearity, where the 3D fundamental solitons are stable, their spinning counterparts are destroyed by oscillatory azimuthal perturbations [20]. However, the square-shaped Q2D lattice, while breaking the rotational invariance of Eq. (1), may also remove the azimuthal instability, as shown by the numerical results presented below.

Eventually, the comparison with numerical results demonstrates that the VK criterion turns out to be *sufficient* for all solitons in the present model. Of course, we here apply the criterion not to exact families of soliton solutions, but rather to the respective VA; however, comparison of the VA predictions for the fundamental-soliton family (Fig. 1) with numerical results reported in Refs. [5–7] and their extensions demonstrates that the VA provides for a very accurate description of the fundamental-soliton family (as was already concluded, in a less detailed form, in Ref. [5]). Comparison with the numerical findings for $S=1$ (see below) demonstrates that the agreement with the VA is good in this case too, although poorer than for $S=0$.

Plots similar to those in Figs. 1 and 2 were also generated for $S\geqslant 2$. They are not displayed here, as they are not borne out by numerical results (which are displayed below for $S=2$).

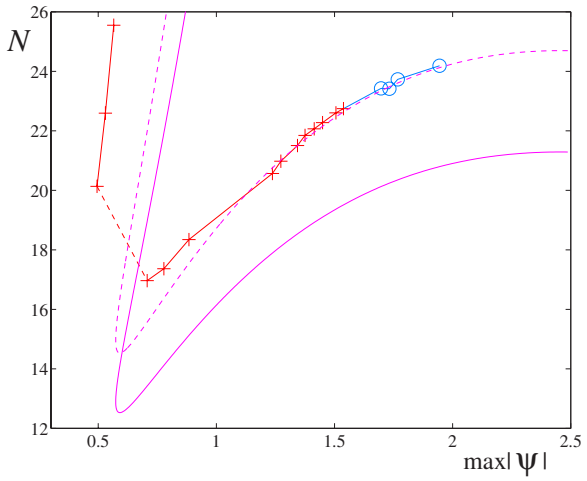

FIG. 3. (Color online) Relations between the norm and amplitude for vortex solitons with $S=1$, found from the numerical solution of Eq. (1). Red crosses and blue circles depict, respectively, stable and unstable vortices, while lines connecting these symbols are only guides for the eye. The continuous line shows the same relation as predicted by the variational approximation based on ansatz (4). The dashed line is a fit to the numerical data, obtained from the variational curve by linear compression, $N \to 1.16N$.

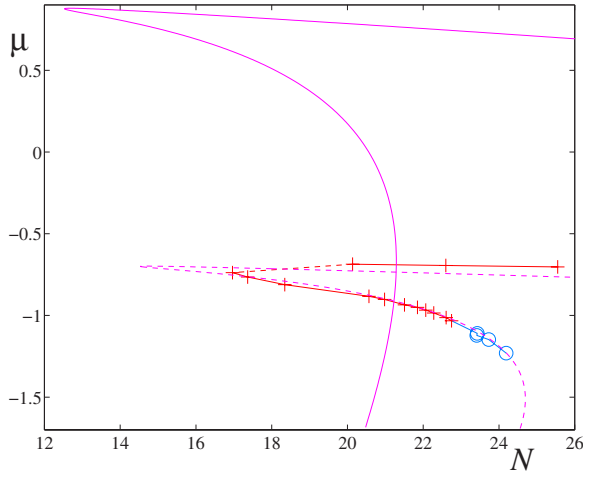

FIG. 4. (Color online) Chemical potential μ versus the norm of vortex solitons with $S=1$. The symbols have the same meaning as in Fig. 3. The dashed line is deduced from the solid one, which is generated by the variational approximation, by a phenomenological linear transformation, $N \to 1.16N$, $\mu \to -1.16+0.525\mu$.

Besides the simplest ansatz, based on Eq. (4), for vortices with $S=1$ we also tried a more sophisticated one, which takes into regard that some of stable solitons of this type are actually composed of four distinct density peaks forming a rhombus (in the 2D model on the 2D lattice, this fact was explicitly used to compose vortex solitons in Ref. [17]). The accordingly constructed ansatz is

$$\psi = \psi_0(x-a,y,z) + i\psi_0(x,y-a,z) - \psi_0(x+a,y,z) - i\psi_0(x,y+a,z), \tag{5}$$

where ψ_0 is the same trial function as in Eq. (4) with $S=0$, the phase distribution in Eq. (5) precisely corresponds to the phase circulation of 2π around the center of the vortex [the center is set at $(x,y)=(0,0)$], and size a of *vortex rhombus* (5) is a variational parameter too, in addition to A_0, ρ, and h in ψ_0. The VA based on ansatz (5) can be implemented by means of computer-assisted analytical calculations. Eventually, the corresponding variational equations yield results which are not conspicuously different from those based on straightforward ansatz (4) [see the dashed curve in Fig. 2(a)], nor are they essentially closer to numerical findings.

II. NUMERICAL RESULTS

A. Computational methods

Stationary 3D solutions of Eq. (1) in the form of vortex solitons, with $S=1$ and $S=2$ (solutions with $S=0$ were obtained in Refs. [6,5]) were constructed by means of a two-step procedure. First, we used the known method of the imaginary time integration [26], starting from the initial ansatz,

$$\psi_{\text{in}}^{(S)} = A(x+iy)^S \exp[-(\sqrt{x^2+y^2}-r_0)^2/(2\rho^2) - z^2/(2h^2)],$$

with values of r_0, ρ, and h chosen to ensure the convergence of the scheme. As in Ref. [6], the Crank-Nicholson method was employed for the integration; in doing so, equations of the implicit scheme were solved using a double Picard iterative procedure. The latter was implemented by resolving the linear system at each step by dint of the Gauss-Seidel iterations.

The accuracy of the stationary solutions produced by the imaginary-time integration was assessed by means of a convergence measure,

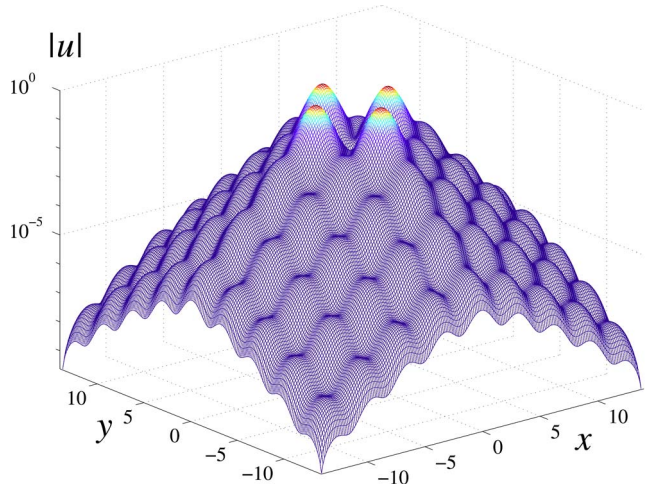

FIG. 5. (Color online) The local amplitude of the wave field in the vortex soliton with $S=1$, in the transverse plane, is shown on the logarithmic scale. A three-dimensional image of this soliton is displayed below in Fig. 8(a).

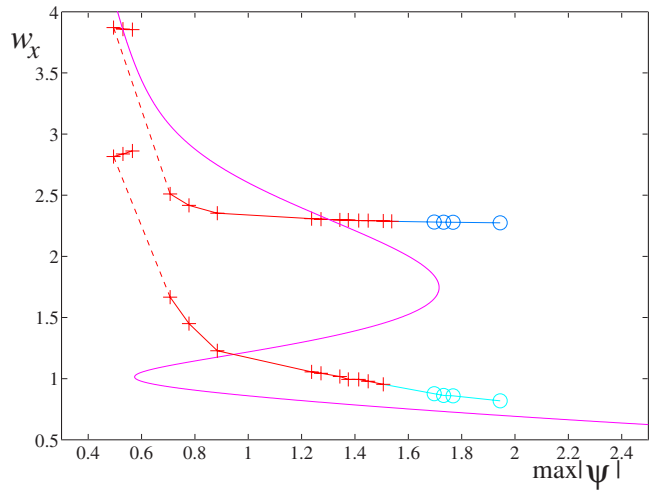

FIG. 6. (Color online) Transverse width w_x of the vortex solitons with $S=1$ versus its maximum amplitude. The symbols have the same meaning as in Fig. 3. The upper and lower sets of the points represent, respectively, the average width, computed as per Eq. (7), and the asymptotic width, as given by Eqs. (10) and (9). The continuous curve is the prediction of the variational approximation, given by Eq. (11).

$$\frac{\max|\psi_{n+1}(x,y,z) - \psi_n(x,y,z)|}{\max|\psi_{n+1}(x,y,z)| + \max|\psi_n(x,y,z)|}, \tag{6}$$

where n is the iteration number, and the maximum is taken over the entire 3D space. For the solutions generated by the first step of the numerical procedure, measure (6) could not be usually made essentially better than 10^{-2} (further continuation of the iterations would lead to a divergence).

At the second step, more accurate stationary solutions were obtained as follows. The Picard iterations lead to the linear system

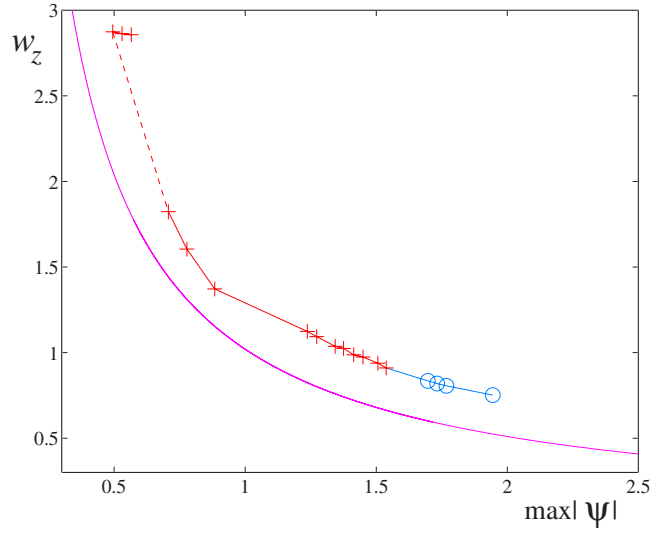

FIG. 7. (Color online) Axial length w_z of the solitons with $S=1$. The symbols and continuous curve represent, respectively, numerical results as given by Eq. (7), and the prediction of the variational approximation as per Eq. (11).

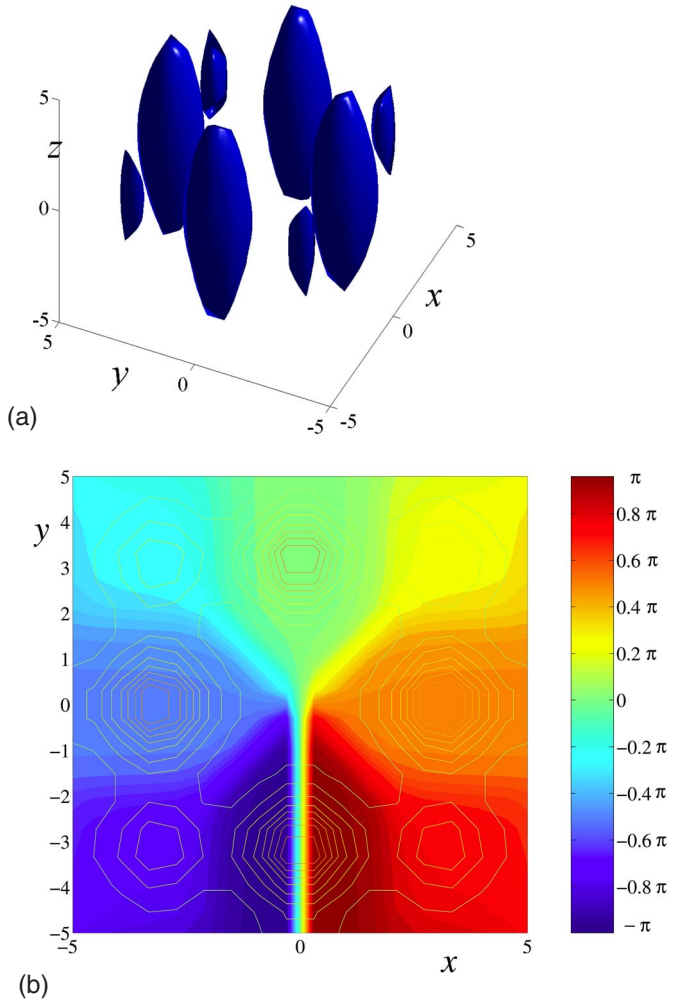

FIG. 8. (Color online) The shape of a stable vortex soliton with $S=1$ belonging to the middle point of the upper branch in Fig. 3 (max$|\psi|=0.53$, $\mu=-0.69$, $N=22.6$): (a) the three-dimensional distribution of the local amplitude $|\psi(x,y,z)|$; (b) the phase distribution, on top of contour plots of the amplitude, in the midplane $z=0$.

$$\psi_{n+1} = -\frac{(1/2)\delta\psi_{n+1} + \omega\psi_{n+1} + \psi_{n+1}|\psi_n|^2}{\mu - \omega - \varepsilon[\cos(2x) + \cos(2y)]},$$

(n is iteration's number), which was solved by means of a fixed-point algorithm, adjusting the value of parameter ω to improve the convergence. Laplacian $\Delta\psi_{n+1}$ was computed using the five-point finite-differences formula along each axis. At this step of the numerical solution, the convergence measure given by Eq. (6) was used again. The computations were performed, typically, in the integration domain of size $-14 \leqslant x,y,z \leqslant +14$, with up to $210\times210\times210$ discretization points. This rather complicated procedure was necessary due to peculiarities of the numerical problem, for which straightforward schemes failed to converge.

After having found the stationary solutions, their stability has been tested by simulating the evolution in real time, using the same Crank-Nicholson method as for the imaginary-

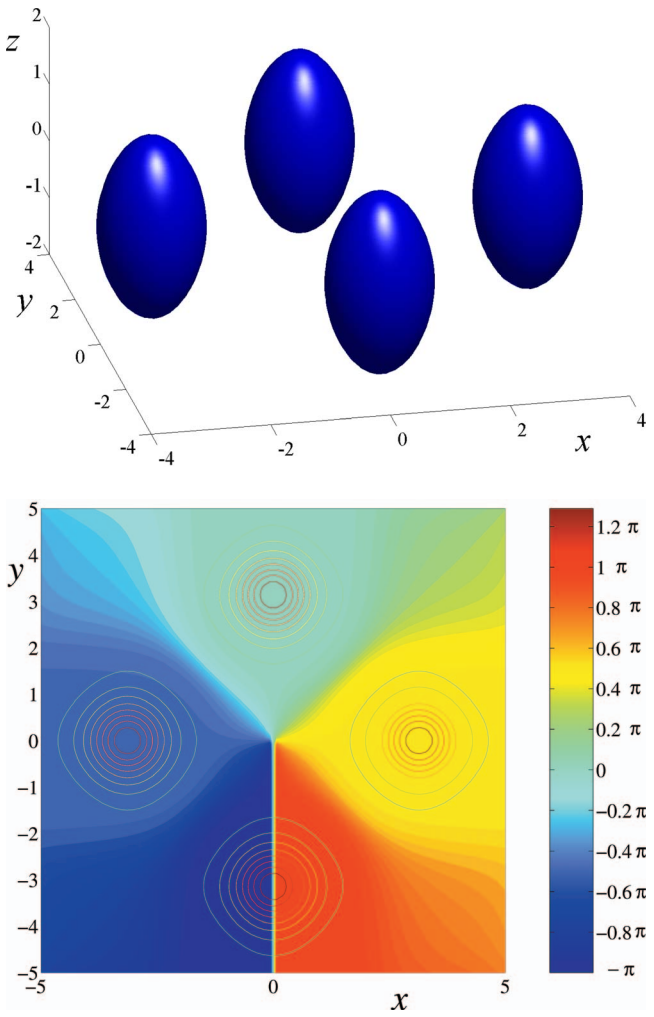

FIG. 9. (Color online) The same as in Fig. 8, but for a stable vortex with a higher amplitude ($\max|\psi|=1.45$, $\mu=-0.98$, $N=22.3$).

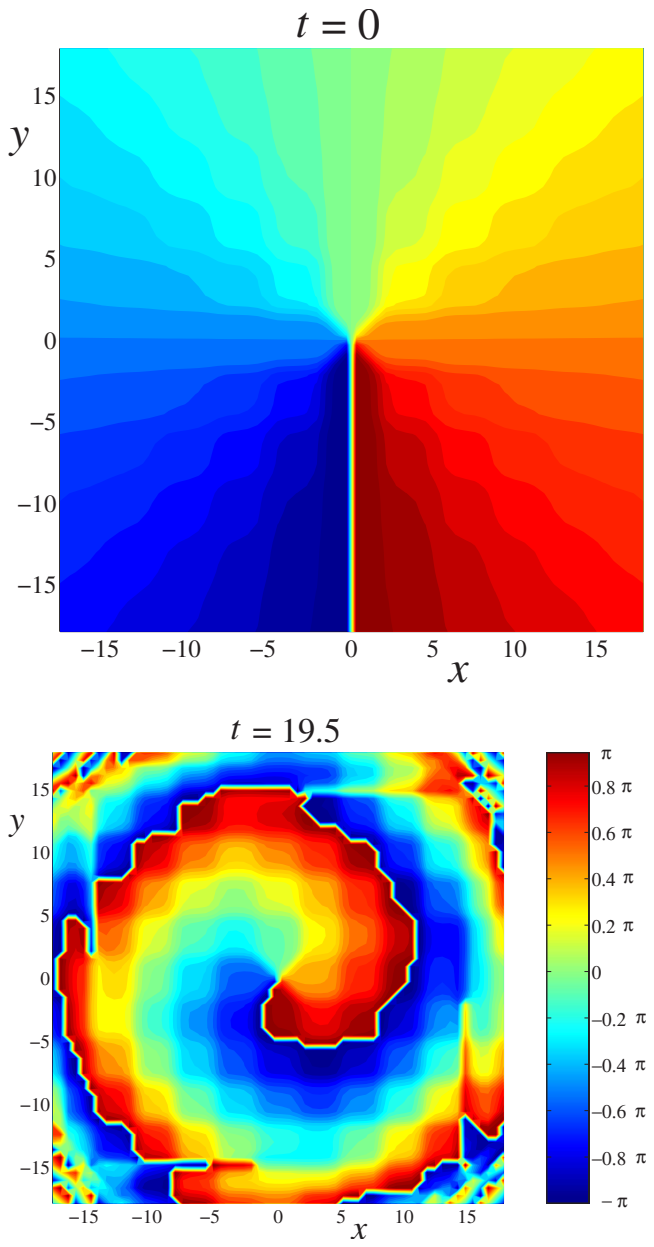

FIG. 10. (Color online) Development of a spiral phase pattern as a result of the decay of a strongly perturbed stable vortex soliton with $S=1$, $\max|\psi|=0.53$, $\mu=-0.69$, and $N=22.6$.

time integration. The initial configuration was a perturbed stationary state, which was either the above-mentioned low-accuracy one produced by the first step of the numerical procedure, or a higher-accuracy state to which a random noise of relative amplitude 0.01 was explicitly added. The real-time integration has confirmed that the accuracy of the stationary states achieved with the two-step procedure was sufficient to find stable vortex solitons.

B. Vortices with $S=1$

The numerical analysis demonstrates that most of the 3D vortex solitons with $S=1$ are stable. Characteristics of this numerically found solution family, in the form of a relation between the norm and amplitude (maximum value of $|\psi(x,y,z)|$) are collected in Fig. 3, which also shows the prediction provided by the VA [for ansatz (4) with $S=1$, $\max|\psi_1|=A\rho/\sqrt{e}$]. Qualitative agreement between the variational and numerical results is observed, which may be improved by a phenomenological linear adjustment of the VA-generated plot (see the dashed curve in Fig. 3). The VA predicts that parts of the solution family corresponding to the rising branches of curve $N=N(\max|\psi|)$, in the interval of $12.53<N<21.29$ for the lower branch, and up to $N=132.6$ for the upper one (only a small part of the latter branch is displayed in Fig. 3), are stable in the sense of the VK criterion. Relations between chemical potential μ and the amplitude are displayed in Fig. 4. It is seen that good agreement between the numerical and variational results can be achieved if the variational plot is linearly adjusted, as stated in the caption to Fig. 4.

The average transverse width and axial length of the axisymmetric 3D soliton, centered at the origin, can be computed numerically as

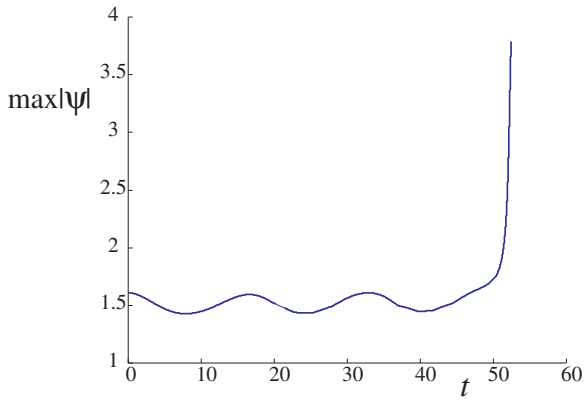

FIG. 11. (Color online) Slow transition to collapse in a quasistable vortex with $S=1$, $\max|\psi|=1.61$, $\mu=-1.30$, and $N=22.89$. In this case, the soliton period may be estimated as $(\max|\psi|)^{-2}\sim 0.4$ (in the normalized units), hence the quasisoliton survives over ~ 125 periods. The shape of this soliton is four peaked (cf. Fig. 9), with all peaks developing the collapse simultaneously.

$$w_x^2 = w_y^2 \equiv w_r^2/2 = \frac{\int x^2|\psi|^2 dxdydz}{\int |\psi|^2 dxdydz}, \quad w_z^2 = \frac{\int z^2|\psi|^2 dxdydz}{\int |\psi|^2 dxdydz}. \tag{7}$$

Another definition of the soliton's size is based on its asymptotic form far from the center, by drawing $|\psi|$ on the logarithmic scale (see Fig. 5) [Gaussian ansatz (5) does not apply to the description of the asymptotic form]. The exponential decay can be fitted to the following expression:

$$\ln(|\psi(x,y,z)|) \approx -\lambda\sqrt{x^2+y^2+\alpha z^2} + \beta[\cos(2x)+\cos(2y)]. \tag{8}$$

Comparison of Eq. (8) to numerical data demonstrates that β slightly varies along the set of data. Decay rate λ can be evaluated numerically as

$$\lambda = -\frac{\int_S \ln(|\psi(x,y,z)|)dxdy}{\int_S \sqrt{x^2+y^2}dxdy}, \tag{9}$$

where S is the domain of the numerical integration in plane $z=0$. The transverse width related to the asymptotic form of the soliton is expressed in terms of λ as

$$w_x = \sqrt{3}/(2\lambda). \tag{10}$$

Numerical results for the soliton's transverse width and axial length are collected in Figs. 6 and 7, respectively. The figures also include the VA prediction for these characteristics of the soliton, which are obtained by the substitution of ansatz (5) in Eqs. (7),

$$w_x^{(\mathrm{VA})} = \rho, \quad w_z^{(\mathrm{VA})} = h/\sqrt{2}. \tag{11}$$

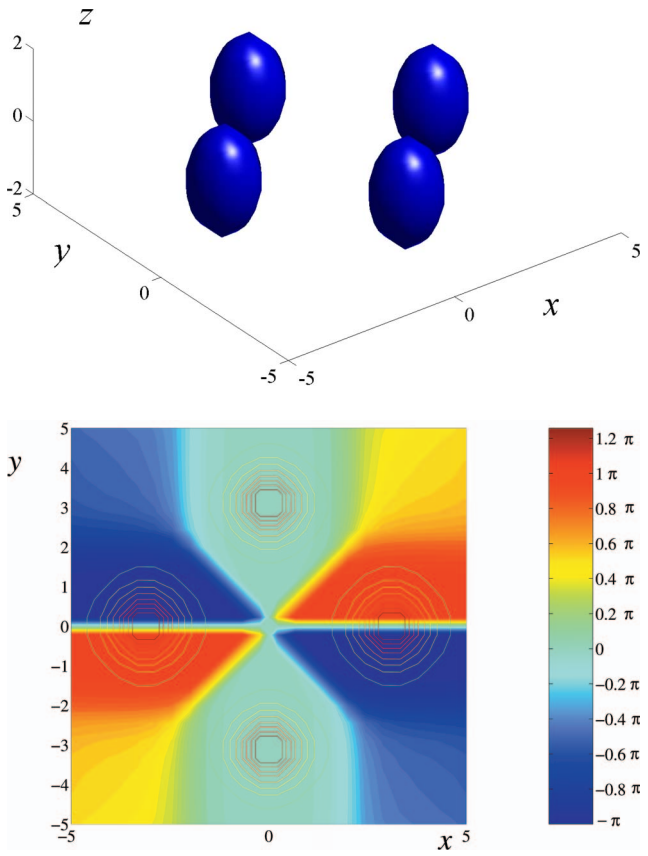

FIG. 12. (Color online) A typical example of the stable vortex soliton with $S=2$, cf. Fig. 9 for $S=1$. In this case, $\varepsilon=-1.25$, $\max|\psi|=1.41$, $\mu=-1.11$, and $N=22.64$.

The figures demonstrate good agreement between the numerical and variational results for w_z. The prediction of the VA for the transverse width is less accurate, but it makes sense too.

The numerical data reveal a gradual transition between two different shapes of the vortex shape, four-peak and eight-peak ones, typical examples of which are displayed in Figs. 8 and 9. The phase around each peak is nearly constant, while the phase difference between the peaks is $\pi/2$ and $\pi/4$, in the former and latter cases, respectively. Additional peaks with lower intensities also exist, as seen from Fig. 5.

Unstable vortices of the same type, with $S=1$, frequently assume the four-peak shape, similar to that in Fig. 9. In most cases, the instability is radial, rather than azimuthal: each peak develops intrinsic collapse, without tangible breakup of the symmetry between them; nevertheless, in some cases the symmetry between the peaks may be broken in the course of the collapse, with a particular peak reaching the singularity first.

The stability margin of the stable vortices is not very large, and a strong enough perturbation may lead to their destruction. A typical example of decay (spreading out due to the diffraction) of a strongly disturbed multipeaked vortex state, belonging to the upper branch in Fig. 3, is displayed in Fig. 10. The phase pattern changes in the course of the decay, developing a spiral form. In this case, the strongly pertubed state has the same global shape and peak amplitude as the unperturbed vortex, but a lower norm.

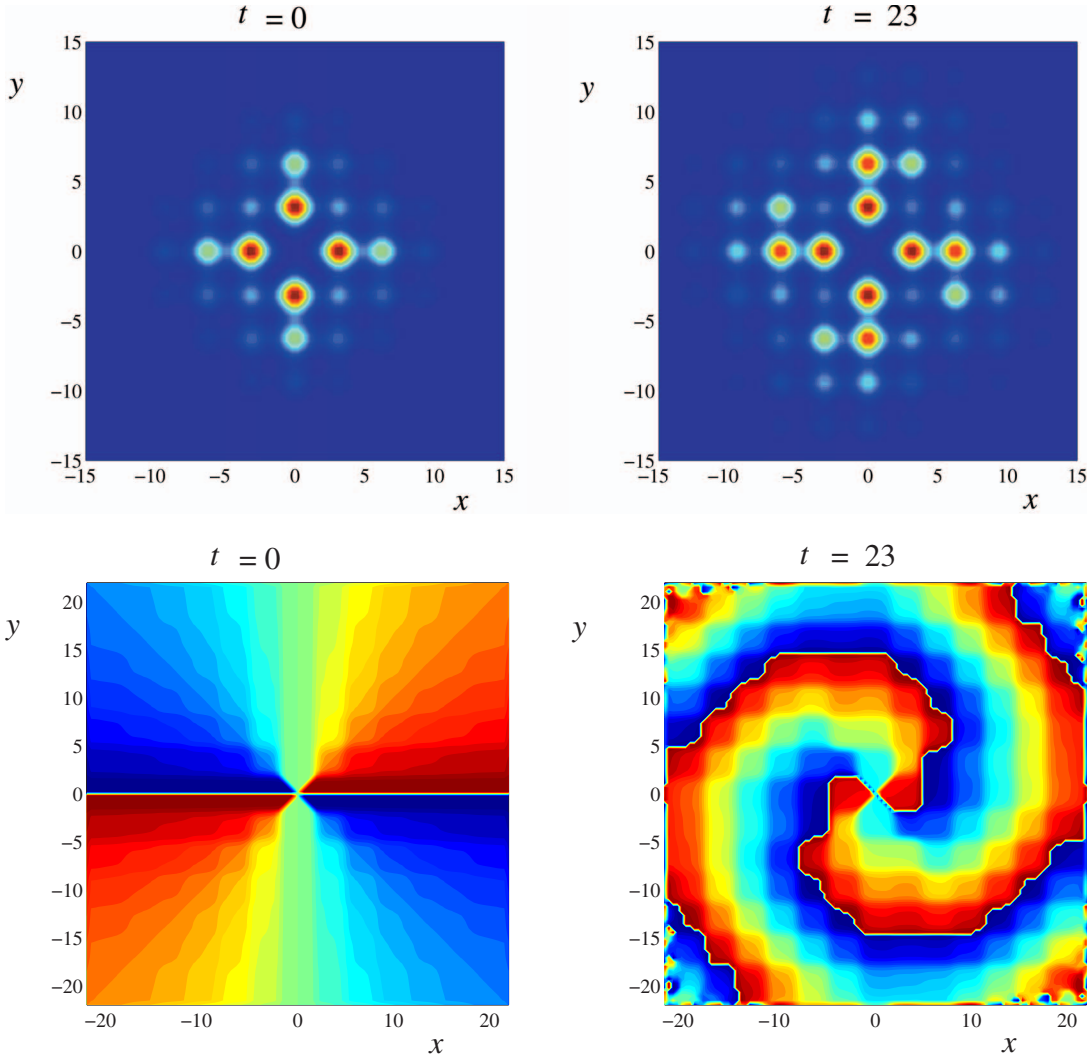

FIG. 13. (Color online) An example of the decay of an unstable vortex soliton with $S=2$, shown by means of intensity plots for $|\psi(x,y)|$ (top), and phase patterns (bottom) in the midplane, $z=0$. In this case, $\varepsilon=-1.25$, and parameters of the unstable soliton are $\max|\psi|=0.25$, $\mu=-0.60$, and $N=5.51$.

Besides the stable vortex solitons with $S=1$ and their definitely unstable counterparts, simulations reveal the existence of objects that may be called *quasistable* pulsating vortices. Generally speaking, they are unstable, but with a slowly developing instability, the onset of which is preceded by several cycles of long-period oscillations, as shown in Fig. 11. These quasistable solitons eventually undergo collapse, as is also seen in Fig. 11, but with a survival time $\gtrsim 100$ soliton periods (the period is a characteristic time of the intrinsic evolution of a stable perturbed soliton). In terms of BEC, it translates into many seconds, hence the quasistable vortex has a good chance to be created in the experiment.

C. Vortices with $S=2$

Numerical analysis produces stable solitons with the double vorticity too. Although their parameters are poorly predicted by the VA, unlike the solitons with $S=1$, Fig. 12 shows that their general structure is again based on four density peaks surrounding an empty site of the OL, the phase shift between the peaks being π. A noticeable difference from their $S=1$ counterparts is that the solitons are stronger localized ("shorter") in the free direction z.

Unstable vortices with $S=2$ are more prone to decay in the lattice's plane (rather than to intrinsic collapse of each individual peak, which may be plausibly explained by stronger repulsion between the peaks with the phase difference of π), in comparison with the unstable vortices that have $S=1$. A typical example of the decay is displayed in Fig. 13, which also features formation of a spiral phase pattern (cf. Fig. 10).

In addition to the intrinsic collapse and decay, a third instability mode was found for the $S=2$ vortices, namely, their decay (self-stretching) in the free direction z. An example of this mode is shown in Fig. 14.

III. CONCLUSION

We have constructed stable three-dimensional solitons with embedded vorticity, $S=1$ and 2, in the three-dimensional Gross-Pitaevskii or nonlinear Schrödinger equa-

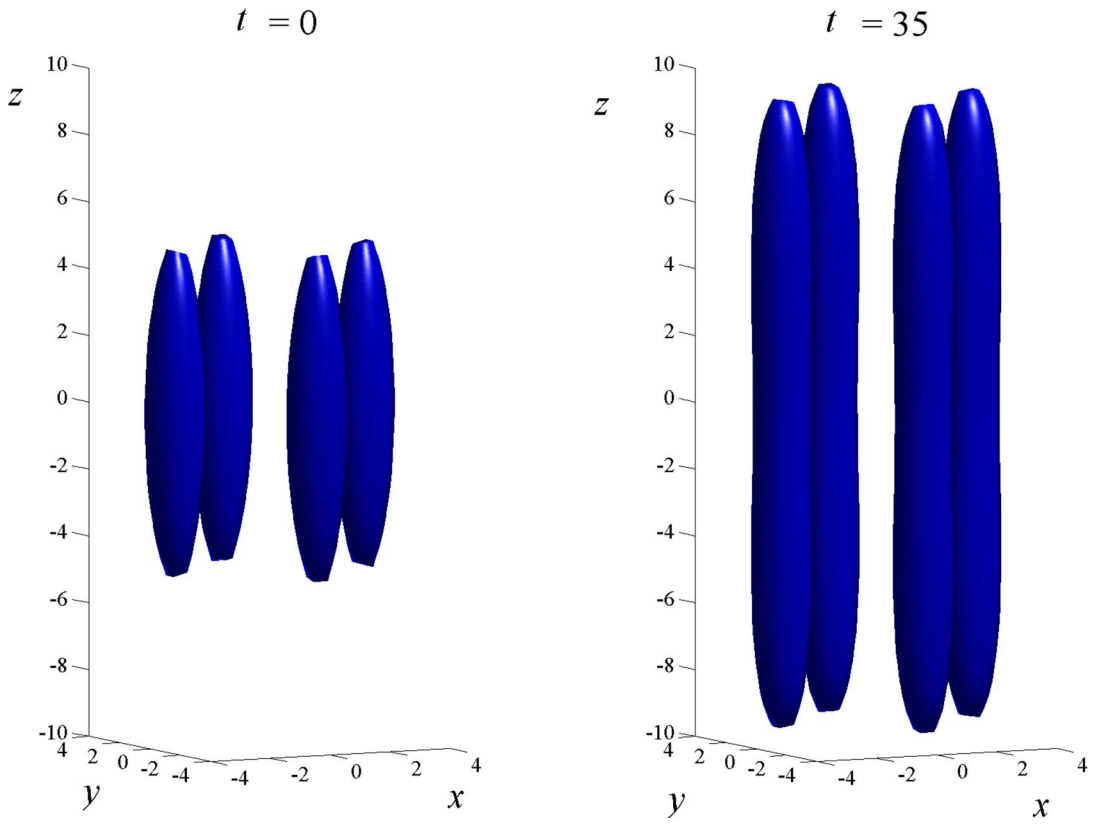

FIG. 14. (Color online) Decay of an unstable vortex with $S=2$ through its indefinite self-stretching in direction z. Parameters are $\varepsilon=-1.25$, $\max|\psi|=0.25$, $\mu=-0.21$, and $N=2.25$.

tion with the quasi-2D square-lattice potential. The model directly applies to BEC with self-attraction trapped in a quasi-2D optical lattice, and, less accurately, to optical spatiotemporal solitons in photonic-crystal fibers. The results provide examples of soliton species that were not reported in previously studied models, viz., stable 3D vortex solitons with $S>1$, and vortex solitons (with any $S\neq 0$) supported by a lattice in the 3D space. The solitons with $S=1$ were predicted by means of the VA (variational approximation), and then found in the numerical form. A special two-stage numerical procedure was developed, which makes it possible to construct the 3D vortices with high accuracy. For the solitons with $S=2$, the VA does not produce relevant results, but stable solitons of this type have been found too, by means of numerical methods. Basically, the localized vortices are built as sets of four fundamental solitons forming a rhombus, with phase shifts $\pi S/2$ between its adjacent sites, and an empty site in the middle. The very possibility of the stability of such patterns in the quasi-2D lattice potential is counterintuitive (as explained in the Introduction), but they exist, nevertheless.

Typical scenarios of the instability development of unstable localized vortices have been identified too. These include simultaneous intrinsic collapse of the four density peaks that constitute the vortex, or, on the contrary, decay of the pattern in the lattice's plane ($z=0$). In the case of $S=2$, an additional instability scenario occurs, namely, self-stretching of the vortex in the orthogonal (unconfined) direction.

With presently available techniques, it is possible to implement predictions of this work in experiments with self-attractive BEC. Experimental creation of "light bullets" with intrinsic vorticity in a photonic-crystal fiber may be possible too. To that end, one may couple into the fiber a femtosecond pulse with the vortical structure created in it by passing through a specially designed mask (cf. Ref. [27]).

ACKNOWLEDGMENTS

The work of B.A.M. was supported, in part, by the Israel Science Foundation through Center-of-Excellence Grant No. 8006/03, and by the German-Israel Foundation through Grant No. 149/2006.

[1] L. Bergé, Phys. Rep. **303**, 260 (1998).
[2] O. Morsch and M. Oberthaler, Rev. Mod. Phys. **78**, 179 (2006).
[3] B. B. Baizakov, B. A. Malomed, and M. Salerno, Europhys. Lett. **63**, 642 (2003).
[4] J. Yang and Z. H. Musslimani, Opt. Lett. **28**, 2094 (2003); Z. H. Musslimani and J. Yang, J. Opt. Soc. Am. B **21**, 973 (2004).

[5] B. B. Baizakov, B. A. Malomed, and M. Salerno, Phys. Rev. A **70**, 053613 (2004).

[6] D. Mihalache, D. Mazilu, F. Lederer, Y. V. Kartashov, L.-C. Crasovan, and L. Torner, Phys. Rev. E **70**, 055603(R) (2004).

[7] B. B. Baizakov, M. Salerno, and B. A. Malomed, in *Nonlinear Waves: Classical and Quantum Aspects*, edited by F. Kh. Abdullaev and V. V. Konotop (Kluwer Academic Publishers, Dordrecht, 2004), p. 61; also available at http://rsphysse.anu.edu.au/~asd124/Baizakov_2004_61_NonlinearWaves.pdf; H. Sakaguchi and B. A. Malomed, Phys. Rev. E **74**, 026601 (2006).

[8] M. Trippenbach, M. Matuszewski, and B. A. Malomed, Europhys. Lett. **70**, 8 (2005); M. Matuszewski, E. Infeld, B. A. Malomed, and M. Trippenbach, Phys. Rev. Lett. **95**, 050403 (2005).

[9] B. A. Malomed, *Soliton Management in Periodic Systems* (Springer, New York, 2006).

[10] D. Mihalache, D. Mazilu, F. Lederer, B. A. Malomed, Y. V. Kartashov, L.-C. Crasovan, and L. Torner, Phys. Rev. Lett. **95**, 023902 (2005).

[11] L. Khaykovich, F. Schreck, G. Ferrari, T. Bourdel, J. Cubizolles, L. D. Carr, Y. Castin, and C. Salomon, Science **256**, 1290 (2002); K. E. Strecker, G. B. Partridge, A. G. Truscott, and R. G. Hulet, Nature (London) **417**, 150 (2002).

[12] S. L. Cornish, S. T. Thompson, and C. E. Wieman, Phys. Rev. Lett. **96**, 170401 (2006); L. Khaykovich and B. A. Malomed, Phys. Rev. A **74**, 023607 (2006).

[13] P. Xie, Z.-Q. Zhang, and X. Zhang, Phys. Rev. E **67**, 026607 (2003); A. Ferrando, M. Zacares, P. F. de Cordoba, D. Binosi, and J. A. Monsoriu, Opt. Express **11**, 452 (2003).

[14] J. C. Knight, J. Arriaga, T. A. Birks, A. Ortigosa-Blanch, W. J. Wadsworth, and P. S. Russell, IEEE Photon. Technol. Lett. **12**, 807 (2000).

[15] A. Ferrando, M. Zacares, P. F. de Cordoba, D. Binosi, and J. A. Monsoriu, Opt. Express **12**, 817 (2004).

[16] D. N. Neshev, T. J. Alexander, E. A. Ostrovskaya, Y. S. Kivshar, H. Martin, I. Makasyuk, and Z. Chen, Phys. Rev. Lett. **92**, 123903 (2004); J. W. Fleischer, G. Bartal, O. Cohen, O. Manela, M. Segev, J. Hudock, and D. N. Christodoulides, *ibid.* **92**, 123904 (2004).

[17] H. Sakaguchi and B. A. Malomed, Europhys. Lett. **72**, 698 (2005).

[18] D. Mihalache, D. Mazilu, L.-C. Crasovan, I. Towers, A. V. Buryak, B. A. Malomed, L. Torner, J. P. Torres, and F. Lederer, Phys. Rev. Lett. **88**, 073902 (2002).

[19] D. Mihalache, D. Mazilu, L.-C. Crasovan, I. Towers, B. A. Malomed, A. V. Buryak, L. Torner, and F. Lederer, Phys. Rev. E **66**, 016613 (2002).

[20] B. A. Malomed, D. Mihalache, F. Wise, and L. Torner, J. Opt. B: Quantum Semiclassical Opt. **7**, R53 (2005).

[21] P. G. Kevrekidis, B. A. Malomed, D. J. Frantzeskakis, and R. Carretero-González, Phys. Rev. Lett. **93**, 080403 (2004); R. Carretero-González, P. G. Kevrekidis, B. A. Malomed, and D. J. Frantzeskakis, *ibid.* **94**, 203901 (2005).

[22] B. A. Malomed, Phys. Rev. E **58**, 7928 (1998).

[23] T. Kapitula, P. G. Kevrekidis, and B. A. Malomed, Phys. Rev. E **63**, 036604 (2001); P. G. Kevrekidis, B. A. Malomed, and A. R. Bishop, J. Phys. A **34**, 9615 (2001).

[24] B. A. Malomed, in *Progress in Optics*, edited by E. Wolf (North Holland, Amsterdam, 2002), Vol. 43, p. 71.

[25] N. G. Vakhitov and A. A. Kolokolov, Izv. Vyssh. Uchebn. Zaved., Radiofiz. **16**, 1020 (1973) [Radiophys. Quantum Electron. **16**, 783 (1973)].

[26] M. L. Chiofalo, S. Succi, and M. P. Tosi, Phys. Rev. E **62**, 7438 (2000).

[27] D. V. Petrov, L. Torner, J. Martorell, R. Vilaseca, J. P. Torres, and C. Cojocaru, Opt. Lett. **23**, 1444 (1998).